

## Z radiation off stops at a linear collider

G. Bélanger<sup>1</sup>, F. Boudjema<sup>1</sup>, T.Kon<sup>2</sup> and V . Lafage<sup>3</sup>

1. *Laboratoire de Physique Théorique LAPTH \**  
*Chemin de Bellevue, B.P. 110, F-74941 Annecy-le-Vieux, Cedex, France.*
2. *Seikei University, Musashino, Tokyo 180-8633, Japan.*
3. *High Energy Accelerator Research Organisation, KEK,*  
*Tsukuba, Ibaraki 305-801, Japan.*

### Abstract

We calculate  $e^+e^- \rightarrow \tilde{t}_1\tilde{t}_1Z$  at a linear collider. For large splitting between the two stops the cross-section is sensitive to the value of  $m_{\tilde{t}_2}$  when this particle is too heavy to be directly produced. The results are compared to  $e^+e^- \rightarrow \tilde{t}_1\tilde{t}_1h$

# 1 Introduction

In the minimal supersymmetric standard model (MSSM), the third generation of sfermions plays a special role both from the theoretical and phenomenological point of view. Large mixing in the third generation can induce large splitting between left and right-handed squarks leading in particular to a top squark significantly lighter than other sfermions. With the Higgs, the stop could be the lightest scalar of the MSSM and thus particularly interesting to study at a linear collider where the moderate total energy restricts the number of sparticles that can be directly produced.

A large mixing in the stop sector not only drives the lightest stop mass down but also can induce large couplings between the top squark and the Higgs affecting in many ways the phenomenology of the Higgs. First, radiative corrections due to top and stop can significantly shift the value of the tree-level mass of the Higgs [1, 2]. More importantly, the Higgs signals at LHC-Tevatron could be completely different from what is generally expected in the MSSM with no mixing. The main discovery channel at the LHC, the loop induced direct production  $gg \rightarrow h \rightarrow \gamma\gamma$ , can be severely suppressed [3]. Furthermore one expects modification of the two-photon width of the Higgs and possibly a large cross-section for associated Higgs production  $\tilde{t}_1\tilde{t}_1h$  or  $\tilde{t}_2\tilde{t}_1h$  [4, 5, 6, 7], where  $\tilde{t}_1(\tilde{t}_2)$  is the lightest (heaviest) top squark.

From the theoretical point of view there is also ample motivation for considering scenarios of light third generation sfermions. For example in inverted hierarchy models only sfermions of the third generation are light enough to be accessible at LHC/Tevatron or a future linear collider, all others being above the TeV scale [8, 9]. Even in models where one assumes universality of sfermion masses at a high scale, the degeneracy is lifted once the masses are run down to the weak scale according to the renormalization group equations and a light  $\tilde{t}_1$  is obtained particularly in models with non-negligible trilinear couplings. These models are especially attractive since they solve the supersymmetric flavor problem while preserving the naturalness argument. Another motivation for considering a light stop is the possibility of obtaining electroweak baryogenesis [10].

In scenarios with a light stop, as was pointed out in [11, 12, 13], the stop pair production at a polarized linear collider can provide a measurement of both the stop mass and the mixing angle. Provided sufficient phase space it was also pointed out that the associated production of stops with a Higgs ( $e^+e^- \rightarrow \tilde{t}_1\tilde{t}_1h$ ) could be observable at a high energy linear collider for some region of the parameter space [7, 14]. In fact in the presence of mixing (associated with a large trilinear term  $A_t$ ) and a heavy  $\tilde{t}_2$ , the coupling of the Higgs to  $\tilde{t}_1$  becomes very large. In [14] we advocated using the information from  $\tilde{t}_1\tilde{t}_1h$  combined with the measurement of  $M_h$  to extract the value of  $\tan\beta$  and  $m_{\tilde{t}_2}$

while the  $\tilde{t}_2$  would be too heavy to be directly produced through  $e^+e^- \rightarrow \tilde{t}_1\tilde{t}_2$ . This is possible since to a good approximation we have shown that apart from  $\tan\beta$  the  $\tilde{t}_1\tilde{t}_1h$  vertex depends only the parameters of the stop sector and so do the dominant corrections to  $M_h$ [14]. However when  $\tilde{t}_1\tilde{t}_1h$  is kinematically accessible so is  $\tilde{t}_1\tilde{t}_1Z$ . The latter process also contains a diagram with Higgs exchange and is therefore also sensitive to the value of the  $\tilde{t}_1\tilde{t}_1h$  coupling. The purpose of this paper is to show that although the dependence on the  $\tilde{t}_1\tilde{t}_1h$  coupling is milder than in  $\tilde{t}_1\tilde{t}_1h$  production, the  $\tilde{t}_1\tilde{t}_1Z$  process features in general a larger cross-section and it can provide complementary information on the parameters of the stop sector.

## 2 Stop parameters

The stop sector involves three independent parameters that can be taken as the physical masses of the two squarks and the mixing angle. The stop mass eigenstates are defined through the mixing angle  $\theta_{\tilde{t}}$ , with the lightest stop,  $\tilde{t}_1$ ,

$$\tilde{t}_1 = \cos\theta_{\tilde{t}}\tilde{t}_L + \sin\theta_{\tilde{t}}\tilde{t}_R \quad (2.1)$$

The mixing angle is related to the off-diagonal term of the mass matrix

$$\sin(2\theta_{\tilde{t}}) = \frac{2m_{\tilde{t}_{LR}}^2}{m_{\tilde{t}_1}^2 - m_{\tilde{t}_2}^2} = \frac{-2m_t(A_t + \mu/\tan\beta)}{m_{\tilde{t}_1}^2 - m_{\tilde{t}_2}^2} \quad (2.2)$$

with  $A_t$  the trilinear parameter of the top and  $\mu$  the Higgs mixing parameter.

When only one stop is kinematically accessible as would most likely be the case at the linear collider, stop pair production ( $\tilde{t}_1\tilde{t}_1$ ) allows for the determination of one mass,  $m_{\tilde{t}_1}$ . The cross-section featuring a strong dependence on  $\cos^2\theta_{\tilde{t}}$ , the amount of mixing can also be determined. This can best be done using polarized beams. A precision at the percent level has been estimated for the high-luminosity 500GeV collider.[15]

In the decoupling limit of large  $M_A$ ,<sup>†</sup> it has been shown [14] that the  $\tilde{t}_1\tilde{t}_1h$  vertex depends only on the three parameters of the stop sector together with  $\tan\beta$ ,

$$\begin{aligned} V_{\tilde{t}_1\tilde{t}_1h} &\simeq \frac{g}{M_W} \left( \sin^2(2\theta_{\tilde{t}}) \frac{(m_{\tilde{t}_1}^2 - m_{\tilde{t}_2}^2)}{4} + m_{\tilde{t}_1}^2 \right. \\ &\quad \left. + M_Z^2 \cos(2\beta) \left( \left( \frac{1}{2} - \frac{2}{3} \sin^2\theta_W \right) \cos^2\theta_{\tilde{t}} + \frac{2}{3} \sin^2\theta_W \sin^2\theta_{\tilde{t}} \right) \right) \quad (2.3) \end{aligned}$$

---

<sup>†</sup>See[14] for further discussion on the validity of this approximation

Note that in this approximation, there is no  $\mu$  dependence in the vertex and that the  $\tan\beta$  dependence arises from the small D-term. For both  $\tilde{t}_1\tilde{t}_1Z$  and  $\tilde{t}_1\tilde{t}_1h$  processes, the value of  $\tan\beta$  affects mainly the computation of the Higgs mass.

The vertex almost vanishes when the stop/top contributions cancel each other. This occurs at

$$\sin(2\theta_{\tilde{t}}) \approx \frac{4m_t^2}{m_{\tilde{t}_2}^2 - m_{\tilde{t}_1}^2} \quad (2.4)$$

At small values of  $\sin 2\theta_{\tilde{t}}$ , the  $\tilde{t}_1\tilde{t}_1h$  vertex, up to small D-terms is of the same order as the  $\tilde{t}\tilde{t}h$  vertex since it is dominated by the  $m_t^2$  term in 2.3. For large values of the  $\tilde{t}_1\tilde{t}_1h$  vertex, the cross section for  $e^+e^- \rightarrow \tilde{t}_1\tilde{t}_1Z$  gets quite large. This occurs for maximal mixing,  $\sin 2\theta_{\tilde{t}} \approx 1$ , with a large splitting between the two stop physical masses,  $m_{\tilde{t}_2} \gg m_{\tilde{t}_1}$ . However it is precisely for this configuration that one has some strong constraints. These will be discussed in the next section.

### 3 Constraints from $M_h$ , $\Delta\rho$ and CCB

The most stringent constraint generally arises from  $\Delta\rho$  which receives contributions from both sbottom and stops. When there is a large splitting between the masses of squarks, the contribution to the gauge-boson self energies becomes sizable and grows with the mass of the heavier squark. The soft-breaking mass,  $m_{\tilde{Q}_L}$ , being common to the two members of the SU(2) doublet, one parameter of the sbottom sector is related to that of the stop sector:

$$m_{\tilde{Q}_L}^2 = \cos^2\theta_{\tilde{t}}m_{\tilde{t}_1}^2 + \sin^2\theta_{\tilde{t}}m_{\tilde{t}_2}^2 - m_t^2 - M_Z^2 \cos(2\beta)\left(\frac{1}{2} - \frac{2}{3}s_W^2\right) \quad (3.5)$$

$$= \cos^2\theta_{\tilde{b}_1}m_{\tilde{b}_1}^2 + \sin^2\theta_{\tilde{b}_1}m_{\tilde{b}_2}^2 - m_b^2 - M_Z^2 \cos(2\beta)\left(-\frac{1}{2} + \frac{1}{3}s_W^2\right) \quad (3.6)$$

If we restrict ourselves to the limit of small mixing in the sbottom sector,  $\theta_b = 0$ , we are left with three free parameters among the five parameters of the third generation squark sector. These will be taken as the physical masses of the stops and the mixing angle,  $\theta_{\tilde{t}}$ . In this limit  $\tilde{b}_1 \approx \tilde{b}_L$  and is the only component entering the radiative corrections to  $\Delta\rho$ . The  $\tilde{b}_2$  is now purely  $\tilde{b}_R$  and decouples from the constraints. There are essentially three contributions to  $\Delta\rho$ , which in the limit of small mixing in the sbottom sector simplifies to,

$$\Delta\rho = -\sin^2\theta_{\tilde{t}}\cos^2\theta_{\tilde{t}}f(m_{\tilde{t}_1}, m_{\tilde{t}_2}) + \cos^2\theta_{\tilde{t}}f(m_{\tilde{t}_1}, m_{\tilde{Q}_L}) + \sin^2\theta_{\tilde{t}}f(m_{\tilde{t}_2}, m_{\tilde{Q}_L}) \quad (3.7)$$

where the functions  $f(m_1, m_2)$  include both one- and two-loop corrections and are defined in [16]. They vanish for equal masses.

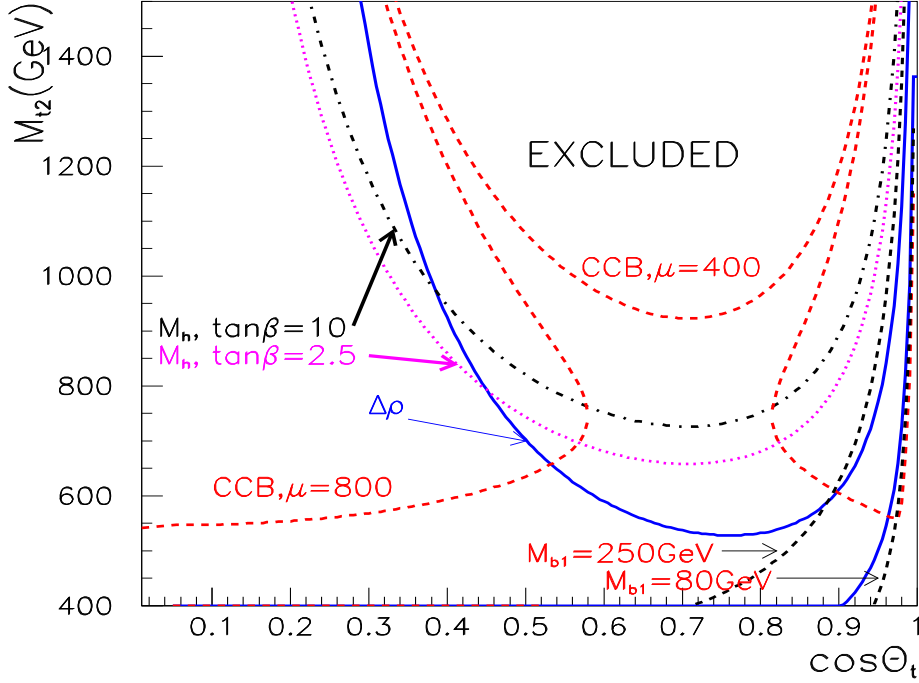


Figure 1: Constraint from  $\Delta\rho \leq 0.0013$  (full line),  $M_h \geq 90\text{GeV}$  (dash-dot), CCB (dash) and  $m_{\tilde{b}_1}$  for  $\tan\beta = 10, \mu = 400\text{GeV}, m_{\tilde{t}_1} = 120\text{GeV}$  and  $M_A = 1\text{TeV}$ . The  $M_h$  constraint for  $\tan\beta = 2.5$  is also shown (dot). The excluded region determined by the above constraints is within the respective boundaries indicated. Note that for  $\cos\theta_{\tilde{t}} \approx 1$ , the  $\Delta\rho$  constraint also excludes the region to the right of the second branch of the  $\Delta\rho$  curve where the present limit on the mass of the sbottom is contained. Requiring sbottom production to be above threshold at a  $500\text{GeV}$  linear collider ( $m_{\tilde{b}_1} \geq 250\text{GeV}$ ) excludes the region to the right of the curve. The CCB constraint for  $\mu = 800\text{GeV}$  is also displayed, the excluded region lies between the two CCB,  $\mu = 800$ , curves.

Imposing the constraint that  $\Delta\rho \leq 0.0013$ [17], we found, as shown in Fig.1, that for large mixing  $\sin 2\theta_{\tilde{t}} \approx 1$ , the large values of  $m_{\tilde{t}_2}$  are ruled out. These results assume a fixed value of  $m_{\tilde{t}_1} = 120\text{GeV}$ . For a near maximal mixing angle, the  $\tilde{t}_2$  cannot exceed  $542\text{GeV}$  while for a mixing  $\cos\theta_{\tilde{t}} \approx .4$  one can allow  $\tilde{t}_2$  up to  $900\text{GeV}$ . When  $\cos\theta_{\tilde{t}}$  is small, ( $\sin 2\theta_{\tilde{t}} \approx 0$ ) masses in excess of  $1\text{TeV}$  are allowed as the contributions from the terms with large mass splittings are damped by the factor  $\sin^2\theta_{\tilde{t}}$ . When  $\cos\theta_{\tilde{t}} \approx 1$  there exist both a lower and upper limit on  $m_{\tilde{t}_2}$ . The region where  $m_{\tilde{t}_2}$  is small corresponds

to one where the common SU(2) squark mass is very low,<sup>‡</sup> all terms give a significant contribution to  $\Delta\rho$ . It is only when  $m_{\tilde{t}_2}$  increases that  $m_{\tilde{Q}_L} \approx m_{\tilde{t}_1}$ , due to the near degeneracy in mass, this term does not contribute to  $\Delta\rho$ . Furthermore there is a near cancellation between the two contributions involving the  $\tilde{t}_2$ .

A large  $\tilde{t}_1\tilde{t}_1h$  vertex also means an important contribution to the Higgs mass. We have taken the approximate formulae at one-loop[18] including a running top mass to incorporate the leading two-loop corrections. In fact the correction to the Higgs mass depends on exactly the same combination of parameters than the one entering the  $\tilde{t}_1\tilde{t}_1h$  vertex[14]. For large mixings and large  $\tilde{t}_2$  mass, the Higgs mass is driven below the present direct experimental limit,  $M_h \leq 90GeV$ , and as the  $\tilde{t}_2$  mass increases is rapidly driven negative. While the value of the Higgs mass is dependent on  $\tan\beta$ , there is only a small shift in the allowed region as  $M_h$  drops very rapidly when the mixing increases. For the region of large  $\sin 2\theta_{\tilde{t}}$ , the constraint from  $\Delta\rho$  is always more stringent, it is only for mixings below  $\approx .4$  that the Higgs mass becomes the most stringent constraint.

One should also mention the constraint arising from the requirement that the parameters do not induce colour and charge breaking global minima (CCB)[19]. An upper bound on  $A_t$ , or on the amount of mixing, follows from this requirement. However it has been argued that the constraints based on the global minima may be too restrictive[20]. It was shown that for a wide range of parameters, the global CCB minimum becomes irrelevant on the ground that the time required to reach the lowest energy state exceeds the present age of the universe. Taking the tunneling rate into account results in a milder constraint which may be approximated[20] by :

$$A_t^2 + 3\mu^2 < 7.5(m_{\tilde{Q}_L}^2 + m_{\tilde{t}_R}^2) \quad (3.8)$$

This constraint depends on  $\mu$  both explicitly and in the calculation of  $A_t$  in terms of physical parameters(see 2.2). For the parameters we are entertaining here, with an intermediate value for  $\mu$ , the mild CCB constraint does not come into effect, it is always superseded by both the  $\Delta\rho$  and  $M_h$  constraints. This value of  $\mu$  was chosen such that there would not be other supersymmetric particles such as gauginos directly produced at the LC. However for large values of  $|\mu|$  this constraint can become very relevant as both an upper limit and a lower limit on  $m_{\tilde{t}_2}$  are obtained. In fact for  $\mu = 800GeV$  the whole area of near maximal mixing is ruled out for any values of  $m_{\tilde{t}_2}$ . Note that in the region near  $\cos\theta_{\tilde{t}} = 1$  the lower bound on  $m_{\tilde{t}_2}$  increases significantly, in this region one obtains negative  $m_{\tilde{Q}_L}^2$  inducing CCB. Both the curves for  $\mu = 400GeV$  and  $800GeV$  are displayed in Fig. 1.

Although the sbottom mass does not enter the calculation of the  $\tilde{t}_1\tilde{t}_1Z$ , one has to

---

<sup>‡</sup>Note that when  $\cos\theta_{\tilde{t}} \approx 1$ , the sbottom mass drops below the direct experimental lower bound.

make sure that the sbottom mass does not drop below the experimental direct bound of roughly 80GeV. This can occur in the region where  $\cos\theta_{\tilde{t}} \approx 1$  especially for the low values of  $m_{\tilde{t}_2}$ . However this constraint is also superseded by the  $\Delta\rho$  constraint, Fig.1. Although not strictly a constraint, we are also interested in knowing whether or not the sbottom is light enough to be directly pair-produced at the linear collider. If such is the case, the direct measurement of its mass, at least in the approximation of small mixing, would be sufficient to completely define the parameters of the stop sector. Note that the region where  $\tilde{b}_1$  is light enough to be pair-produced corresponds to either small  $m_{\tilde{t}_2}$  or  $\cos\theta_{\tilde{t}} \approx 1$ . In either case the  $\tilde{t}_1\tilde{t}_1h$  vertex is not large as seen in Fig.2.

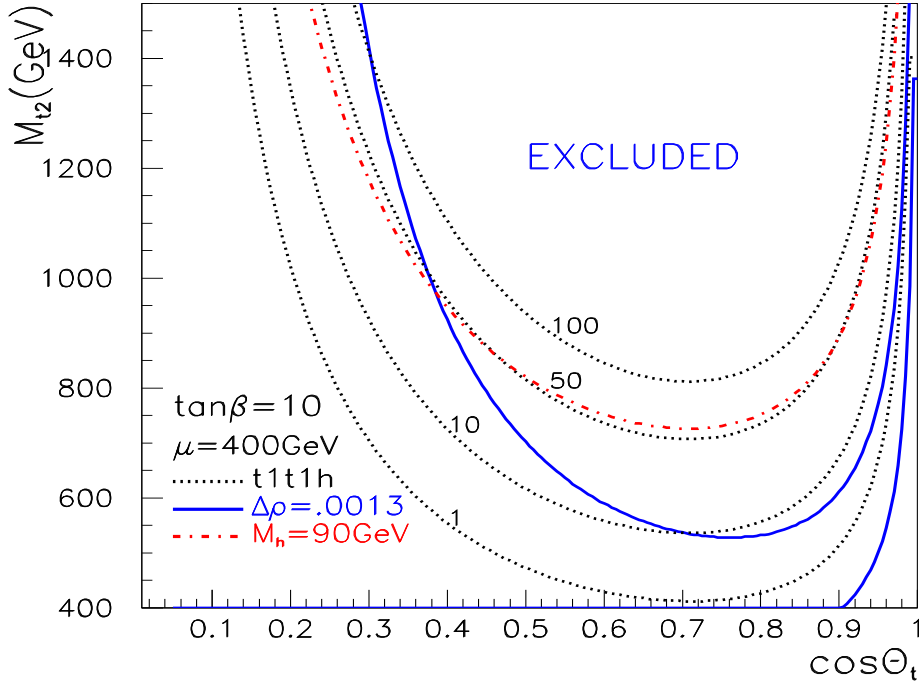


Figure 2: Equipotential lines (dotted) for the normalized coupling  $R_{\tilde{t}_1} = 1, 10, 50, 100$ , see text, with  $\tan\beta = 10$  and  $\mu = 400\text{GeV}$ . The exclusion regions corresponding to  $\Delta\rho \leq .0013$  and  $M_h \leq 90\text{GeV}$  are reproduced from Fig.1.

As we are interested in probing the large Yukawa coupling, it is useful to estimate the strength of the  $\tilde{t}_1\tilde{t}_1h$  coupling before going to the full calculation. To this end we define the coupling squared normalized to the coupling in the no-mixing limit and without a

D-term, this corresponds approximately to the strength of the  $t\bar{t}h$  coupling,

$$R_{\tilde{t}_1} = \left( \frac{M_W V_{\tilde{t}_1 \tilde{t}_1 h}}{g m_{\tilde{t}_1}^2} \right)^2 \quad (3.9)$$

In Fig. 2 we show contour plots for this normalized coupling for  $\mu = 400 GeV$  and  $\tan \beta = 10$ . These curves are based on the exact expression for the vertex (for example see[14]) including the one-loop corrections to the mass and coupling of the Higgs. For clarity the  $M_h$  and  $\Delta\rho$  constraint discussed above are reproduced there as well. In Fig. 2 one sees that  $R_{\tilde{t}_1}$  cannot exceed 50. In fact the equipotential  $R_{\tilde{t}_1} = 50$  almost coincides with the  $M_h \geq 90 GeV$  exclusion curve, thus it is the maximum enhancement of coupling one can hope for. For certain values of the mixing angle,  $\delta\rho$  excludes lower values of  $R_{\tilde{t}_1}$ . For example near the maximal mixing, the  $\Delta\rho$  constraint precludes  $R_{\tilde{t}_1} \geq 10$  while in the large  $\cos \theta_{\tilde{t}}$  region  $R_{\tilde{t}_1}$  could barely exceed 1.

When presenting our results we will, unless otherwise stated, impose the limits  $M_h > 90 GeV, \Delta\rho < .0013$  [21, 17] together with the mild CCB constraint for  $\mu = 400 GeV$ , Eq. 3.8. we also impose a limit on the squark mass,  $m_{\tilde{b}_1} \geq 80 GeV$  [22].

## 4 Results

The calculation was performed with the use of the GRACE-SUSY package for automatic calculation of SUSY processes[23]. We modified the tree-level package to include the important radiative corrections to the Higgs mass and couplings. We have included only one-loop corrections for the third generation squarks. For not too large values of  $\tan \beta$ , the stop contribution completely overwhelms the sbottom contribution. As mentioned above, the relevant parameters are the masses of the stop squarks and the stop mixing angle. The mass of the pseudoscalar is taken to be  $M_A = 1$  TeV while we have chosen  $\mu = 400 GeV$ . The latter parameter in principle enters the  $\tilde{t}_1 \tilde{t}_1 h$  vertex but in effect does not influence much the numerical results. Although the  $\tilde{b}_2$  does not contribute to the  $\tilde{t}_1 \tilde{t}_1 Z$  process, we fixed  $m_{\tilde{b}_2} = 800 GeV$  to ensure that this particle cannot be directly produced even at  $\sqrt{s} = 800 GeV$ . Due to the reduced phase space available at a 500 GeV collider, we have only considered the case  $m_{\tilde{t}_1} = 120 GeV$ . For this mass, the cross-section for  $e^+e^- \rightarrow \tilde{t}_1 \tilde{t}_1 Z$  can vary by more than an order of magnitude from  $\approx .05 fb - 1.5 fb$  depending on the value of the input parameters as well as on the choice of polarisation. Note that this is far from the orders of magnitude variations that we encountered for  $\tilde{t}_1 \tilde{t}_1 h$  production[14]. Fig.3 shows how drastically  $\tilde{t}_1 \tilde{t}_1 h$  changes as  $m_{\tilde{t}_2}$  is varied compared to the mild variation of  $\tilde{t}_1 \tilde{t}_1 Z$ . The main reason for this difference is that  $\tilde{t}_1 \tilde{t}_1 h$  is completely dominated by the  $\tilde{t}_1 \tilde{t}_1 h$  vertex whereas in  $\tilde{t}_1 \tilde{t}_1 Z$  different classes of diagrams contribute, Fig.4. To get a better understanding on the dependence on the input parameters it is



instructive to consider the contribution from each set of diagrams. The crucial point to note is that some diagrams will involve only gauge couplings while others will involve Yukawa couplings. The latter are potentially large in the large mass splitting case.

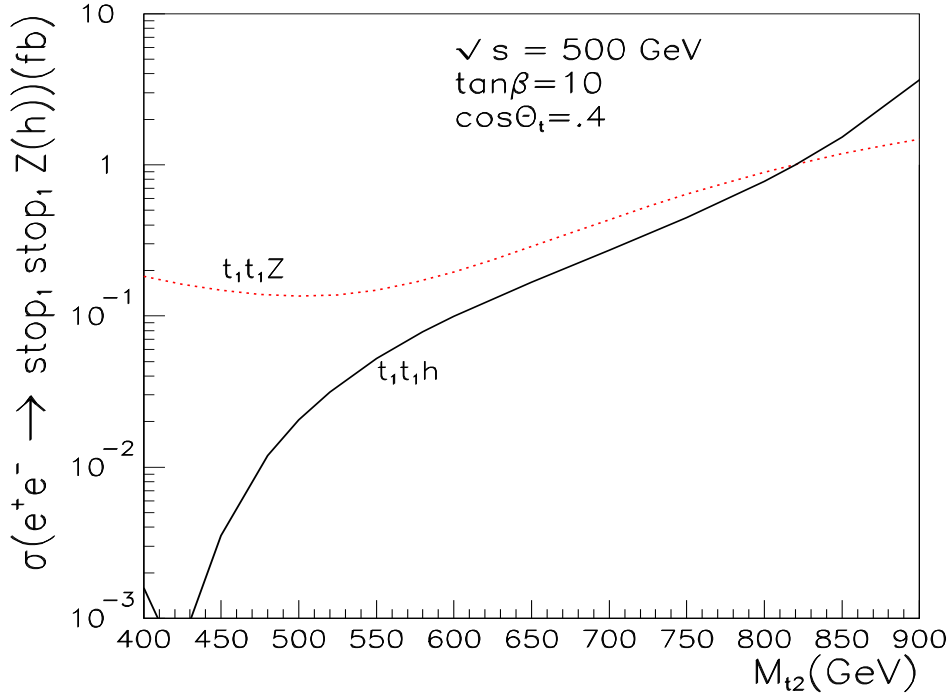


Figure 3: Comparison of  $e^+e^- \rightarrow \tilde{t}_1\tilde{t}_1h$  and  $e^+e^- \rightarrow \tilde{t}_1\tilde{t}_1Z$ . 100% right-handed  $e^-$  polarisation assumed and  $m_{\tilde{t}_1} \approx 120\text{GeV}$ .

There are three classes of diagrams that enter this process, Fig. 4,

- a) Initial state Z radiation.
- b) Final state Z radiation, this includes a diagram with a quartic vertex.
- c) Final state Z radiation with exchange of a  $\tilde{t}_2$ .
- d) Higgs exchange diagrams. These also include a diagram involving the exchange of the heavy Higgs, which however is negligible.

The only diagrams involving the potentially large Yukawa coupling are, besides the Higgs exchange diagram, the ones corresponding to Z radiation off  $\tilde{t}_2$  Fig. 4c). The large

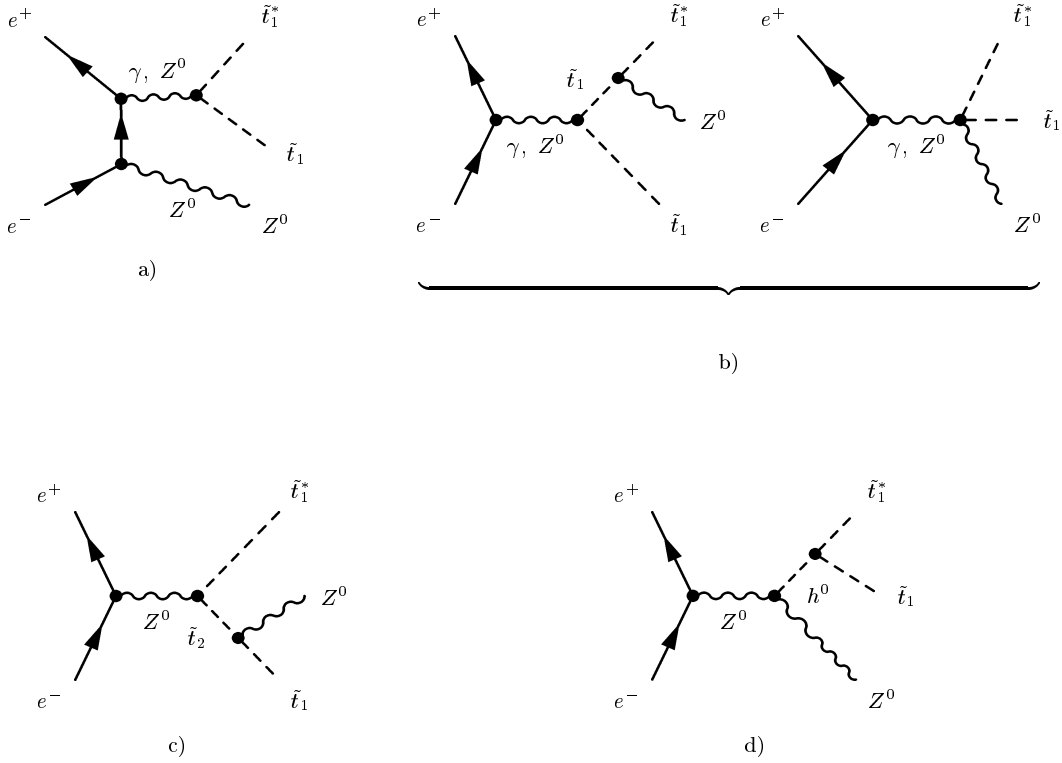


Figure 4: *Classes of Feynman diagrams for  $e^+e^- \rightarrow \tilde{t}_1\tilde{t}_1^*Z$ . a) Initial state radiation b) Final state radiation c) Final state radiation from  $\tilde{t}_2$  d) Higgs exchange*

Yukawa coupling arises from the Goldstone component of the coupling, thus when the splitting is large  $\tilde{t}_2 \rightarrow \tilde{t}_1 Z$  can be approximated by  $\tilde{t}_2 \rightarrow \tilde{t}_1 \phi^0$ ,  $\phi^0$  being the neutral Goldstone Boson, with an effective coupling  $g \frac{1}{4M_W} \sin 2\theta_{\tilde{t}} (m_{\tilde{t}_2}^2 - m_{\tilde{t}_1}^2) = g/2M_W m_t (A_t + \mu/\tan\beta)$ . Nonetheless these diagrams also have a  $\frac{1}{m_{\tilde{t}_2}^2}$  factor from the propagator and we found the overall contribution to the cross-section to be rather small. Only the diagram with Higgs exchange will then feature a Yukawa coupling enhancement, hence a  $m_{\tilde{t}_2}$  dependence through the  $\tilde{t}_1\tilde{t}_1^*h$  coupling. This diagram will contribute to the cross-section according to the strength of the  $\tilde{t}_1\tilde{t}_1^*h$  vertex, from negligible to almost 100%, as Fig. 5 shows. In fact the contribution of this diagram can almost be inferred from the cross-section  $e^+e^- \rightarrow \tilde{t}_1\tilde{t}_1^*h$ , see Fig.3. As for the Z radiation diagrams, they are dominated by the contribution from Z radiation off initial beams (an order of magnitude larger than the Z radiation off stops). They account for  $\sigma = .2fb$  at  $\cos\theta_{\tilde{t}} = 0.4$ . For a collider of luminosity  $\mathcal{L} = 500fb^{-1}$ , this corresponds to over 100 raw events. While these events could be recorded and the cross-section measured, it would not provide any additional information on the value of the unknown parameter of the stop sector, this could be considered as "background" events.

To analyse the  $m_{\tilde{t}_2}$  dependence of the cross-section, first consider the case of interme-

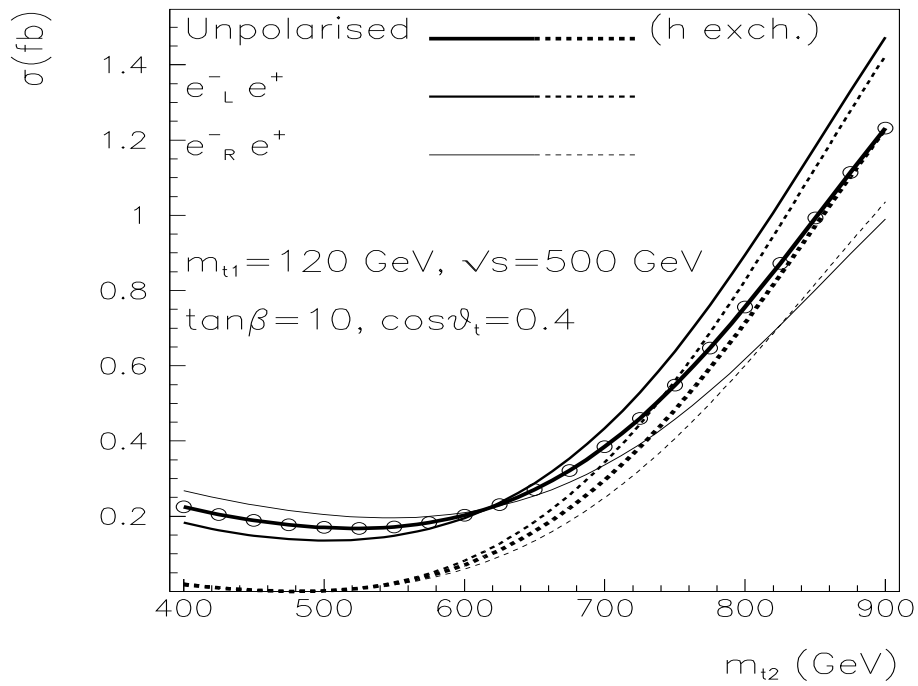


Figure 5: Polarized and unpolarized cross-section for  $e^+e^- \rightarrow \tilde{t}_1\tilde{t}_1Z$ ,  $\cos\theta_{\tilde{t}} = 0.4$ ,  $\tan\beta = 10$  and  $\mu = 400\text{GeV}$ . The contribution of the Higgs exchange diagram is displayed(dash).

mediate mixing, for example  $\cos\theta_{\tilde{t}} = .4$ . As was the case for  $e^+e^- \rightarrow \tilde{t}_1\tilde{t}_1h$ , the cross-section is smallest for  $m_{\tilde{t}_2} \approx 400 - 600\text{GeV}$ , this corresponds to the region where the  $\tilde{t}_1\tilde{t}_1h$  vertex drops significantly. As the  $\tilde{t}_2$  mass increases the cross-section increases significantly by almost one order of magnitude. As reflected in Fig.5, this is essentially due to the rapidly rising contribution from the Higgs exchange diagram, itself driven by the coupling  $\tilde{t}_1\tilde{t}_1h$ . At  $m_{\tilde{t}_2} = 900\text{GeV}$ , the Higgs diagram alone explains the major part of the cross-section, although some important interference effect between the Higgs exchange diagram and all other diagrams remains. In particular there is some small constructive interference between the initial Z bremsstrahlung and the Higgs contribution and a more important (at the 10% level) destructive interference between the final bremsstrahlung and the Higgs exchange diagram. For this particular value of the mixing angle, the various contributions conspire to cancel each other at the highest mass and one is left with a cross-section which seems nearly 100% arising from the  $h$  exchange diagram. This fortuitous cancellation at  $\cos\theta_{\tilde{t}} = 0.4$  does not occur when one looks at the polarised cross-section or at any other value of the mixing angle. Note that this behaviour is in stark contrast with what was obtained for  $e^+e^- \rightarrow \tilde{t}_1\tilde{t}_1h$ . There, whenever the  $\tilde{t}_1\tilde{t}_1h$  vertex vanishes, the cross-section becomes exceedingly small, since the only diagram that does not contain either  $\tilde{t}\tilde{t}h$  vertices, the one originating from  $e^+e^- \rightarrow hZ$  is completely negligible for the whole range of parameters. Indeed, at high energy a longitudinal Z, which is essentially a Goldstone boson, would be mainly produced but this Goldstone boson does not couple to  $\tilde{t}_1\tilde{t}_1$ . On the other hand, in associated Z production, the same  $hZ$  initiated diagram gives a significant contribution to the cross-section as it is now the Higgs accompanying the longitudinal Z that splits into  $\tilde{t}_1\tilde{t}_1$  pairs, and this with a potentially large vertex enhancement.

Next consider the effect of polarisation. While for  $\tilde{t}_1\tilde{t}_1$  pair production the value of the stop mixing angle determined the polarised cross-section, for the  $\tilde{t}_1\tilde{t}_1Z$  process one has to take into account other parameters as well. In the region where the cross-section arises mainly from the diagrams with a Z bremsstrahlung, either initial or final, the polarisation dependence is expected to be similar to the one for stop pair production since essentially gauge couplings, which do not change the chirality are involved. In the latter process, the cross-section is dominated by  $e_R^-$  for  $\cos\theta_{\tilde{t}} \leq .5$  otherwise by  $e_L^-$ . However when the Higgs coupling to  $\tilde{t}_1\tilde{t}_1$  becomes large, which for intermediate or large mixing corresponds to the large  $m_{\tilde{t}_2}$  region, it is the Higgs exchange diagram that is responsible for most of the cross-section, Fig.5. In this case the dominant polarisation configuration is the same as for an s-channel Z production. The ratio of the polarised cross-section is given more or less by the ratio of the couplings of the Z to  $e_L$  and  $e_R$  respectively. Note that the difference between the two polarised cross-sections is not very pronounced for the value of the mixing we have chosen, it is more marked in the case of small mixing,  $\sin 2\theta_{\tilde{t}} \approx 0$ .

Furthermore for large  $\cos\theta_{\tilde{t}}$  one expects  $e_L^-$  to dominate whether or not one benefits from the large Yukawa enhancement. The expectations for different values of  $\cos\theta_{\tilde{t}}$  will be discussed next.

For  $\cos\theta_{\tilde{t}} \approx 0$ ,  $\sin 2\theta_{\tilde{t}} \approx 0$ , one expects from the expression of the  $\tilde{t}_1\tilde{t}_1h$  vertex, Eq. 2.3, a very mild dependence on the  $\tilde{t}_2$  mass, see Fig.6. As a result of the  $m_{\tilde{t}_2}^2$  contribution cancelling against the mixing contribution, as  $\cos\theta_{\tilde{t}}$  increases the strength of the  $\tilde{t}_1\tilde{t}_1h$  vertex decreases until, for  $\cos\theta_{\tilde{t}} = .2$  and  $m_{\tilde{t}_2} = 900GeV$ , there is a precise cancellation between the stop/top term in the vertex. One is then left with only the contribution from the bremsstrahlung diagrams. Only when the mixing becomes significant can one see a rise in the cross-section at large masses. As discussed in the previous section, the  $\Delta\rho$  constraint eliminates the upper range of cross-section as indicated by dots in Fig.6. In fact when mixing reaches  $\cos\theta_{\tilde{t}} = 0.6$ , the maximum value for  $m_{\tilde{t}_2} \approx 600GeV$  and  $\sigma \leq 0.4fb^{\S}$ . For large  $\cos\theta_{\tilde{t}}$ , because of the  $\Delta\rho$  constraint (see Fig.2) one does not benefit from the strong enhancement of the vertex and  $\sigma$  cannot exceed  $0.3fb$ . Furthermore, in these configurations the sbottom is often directly accessible in the pair production process, this is indicated by an arrow in Fig.6. The numerical results confirm what we had anticipated in the previous section, whenever the sbottom can be pair-produced, there is not much interest in the 3-body processes. This point concerns not only the  $\tilde{t}_1\tilde{t}_1Z$  but also  $\tilde{t}_1\tilde{t}_1h$  production as this is just a reflection of the strength of the  $\tilde{t}_1\tilde{t}_1h$  vertex.

The polarised cross-sections follow approximately the same pattern, see Fig. 7. As expected, the  $e_L^-$  is dominant for large  $\cos\theta_{\tilde{t}}$ , the cross-section can reach  $0.75fb$  even for a low mass  $m_{\tilde{t}_2} = 400GeV$  at  $\cos\theta_{\tilde{t}} = .9$ . The same polarisation dominates also for intermediate  $\cos\theta_{\tilde{t}}$  provided  $m_{\tilde{t}_2}$  is large, that is large Yukawa coupling, otherwise the choice of a right handed electron polarisation gives a larger cross-section.

For all numerical results presented we have taken  $m_{\tilde{t}_2} \leq 900GeV$ , the maximum value allowed for  $\cos\theta_{\tilde{t}} = 0.4$ . However one should keep in mind that for smaller values of  $\cos\theta_{\tilde{t}}$ , the “large” Yukawa enhancement of the cross-section occurs for  $\tilde{t}_2$  masses above  $1TeV$  which still passes all constraints, see Fig. 1. Nevertheless for these angles the fluctuations with  $m_{\tilde{t}_2}$  are never dramatic and lie within the  $3\sigma$  interval with a high-luminosity  $\mathcal{L} = 500fb^{-1}$ .

We have already alluded to some of the differences between associated Higgs and associated  $Z$  production. The main point is that one does not expect as sharp a dependence on the  $\tilde{t}_1\tilde{t}_1h$  vertex (that is on  $m_{\tilde{t}_2}$  for a given mixing angle) as the process  $\tilde{t}_1\tilde{t}_1h$  itself since only one diagram contributing to the  $\tilde{t}_1\tilde{t}_1Z$  cross-section involves the Higgs. However as

---

<sup>§</sup> In the maximal mixing region one hits a non-physical region where the Higgs mass is driven negative and the cross-section cannot even be computed, as is the case for example for  $0.42 \leq \cos\theta_{\tilde{t}} \leq 0.88$  when  $m_{\tilde{t}_2} = 900GeV$ .

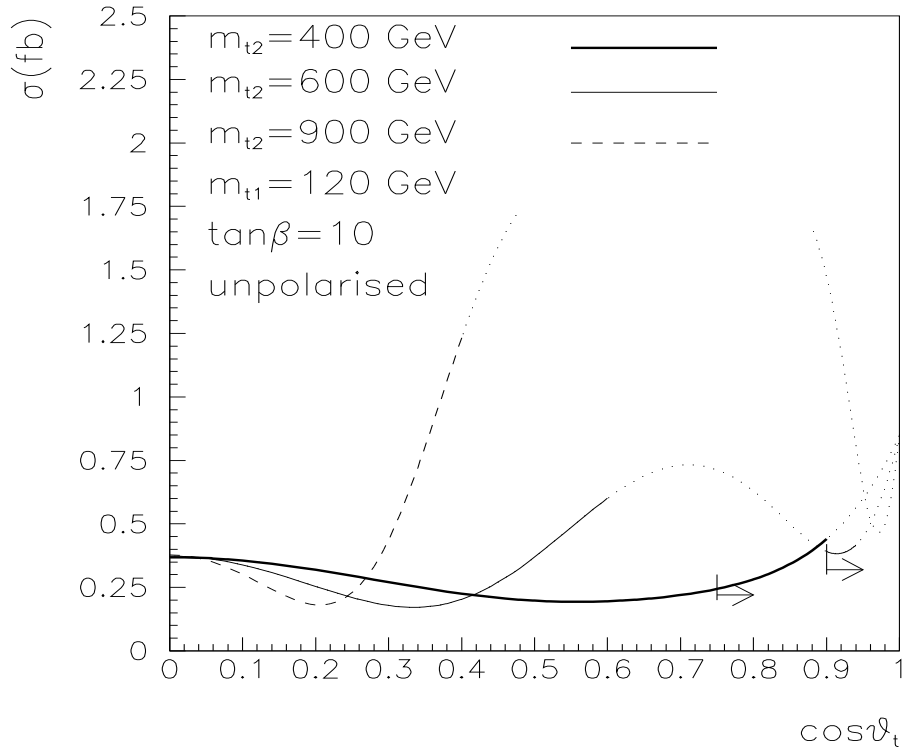


Figure 6:  $\sigma(e^+e^- \tilde{t}_1\tilde{t}_1 Z)$  vs  $\cos\theta_{\tilde{t}}$  for  $m_{\tilde{t}_1} = 120\text{GeV}$   $m_{\tilde{t}_2} = 400, 600, 900\text{GeV}$ . Points that do not pass the constraints are indicated as dots. To the right of the arrows,  $\tilde{b}_1$  pair production opens up ( $m_{\tilde{b}_1} \leq 250\text{GeV}$ ).

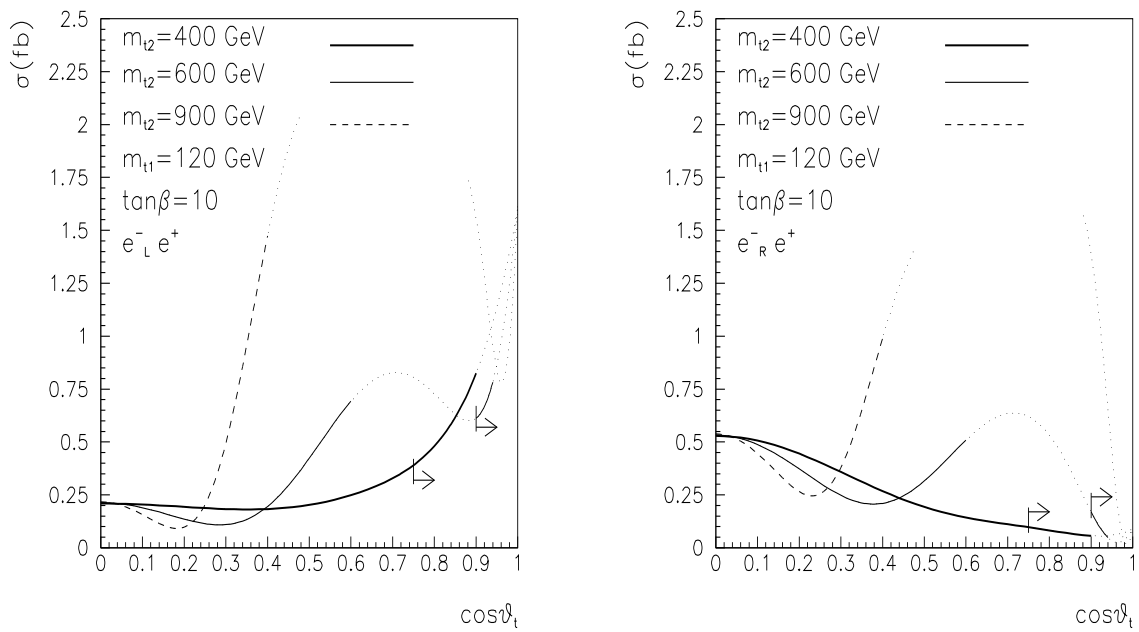


Figure 7:  $\sigma(e^+e^- \rightarrow \tilde{t}_1\tilde{t}_1Z)$  vs  $\cos\theta_{\tilde{t}}$  for  $m_{\tilde{t}_1} = 120\text{GeV}$ ,  $m_{\tilde{t}_2} = 400, 600, 900\text{GeV}$  with polarised beams. The meaning of the dotted lines and the arrows is the same as in the previous figure.

compared to the latter the associated Z channel features a larger cross-section for a large range of parameters. It could therefore be used in conjunction with the associated Higgs channel to help determine the parameters of the stop sector, in particular the mass of the  $\tilde{t}_2$ , Fig. 3. For example, assuming an efficiency of 50% and an intermediate value for  $\sigma = .38fb$  at  $\cos\theta_{\tilde{t}} = .4$  for unpolarised beams one could deduce from a  $3\sigma$  measurement a mass  $m_{\tilde{t}_2} = 700^{+30}_{-50}GeV$ . The uncertainty is of the same order as that expected in  $e^+e^- \rightarrow \tilde{t}_1\tilde{t}_1h$ [14]. For this particular mixing angle, roughly the same precision is expected from either electron beam polarisation.

If the lightest stop turns out not to be so light, one would need to go to higher centre-of-mass energies to observe some events from the associated production of stop and Z. However higher energies can also mean more phase space for the direct production process  $e^+e^- \rightarrow \tilde{t}_1\tilde{t}_2$ . Not only could the direct production of  $\tilde{t}_2$  allow for the determination of  $m_{\tilde{t}_2}$  it can also trigger the final state  $\tilde{t}_1\tilde{t}_1Z$ . This occurs when the  $\tilde{t}_2$  further decays in  $\tilde{t}_1Z$ . Cross-sections of a few  $fb$ s can be reached[24], and the partial width into this mode can be quite large, since the  $\tilde{t}_2 \rightarrow \tilde{t}_1Z_L$  can benefit from the large Yukawa enhancement, as discussed earlier. This branching fraction however depends on the parameters of the MSSM and in particular those of the sbottom sector. We will not entertain this possibility any longer, here we rather consider only values of the two physical stop masses such that  $\tilde{t}_1\tilde{t}_2$  is above threshold. We have considered  $\sqrt{s} = 800GeV$  and different values of  $m_{\tilde{t}_1}$  while varying  $m_{\tilde{t}_2}$  in the range such that  $\tilde{t}_1\tilde{t}_2$  is above threshold. In this case we only see a mild dependence on the  $\tilde{t}_1\tilde{t}_1h$  vertex, and that mostly for the lower values of  $m_{\tilde{t}_1}$ , Fig. 8. At this energy one can hope for a signal only for  $m_{\tilde{t}_1}$  below about 250GeV.

An important issue that remains to be quantified is the detectability of the signal both for the associated Higgs and the associated Z processes. For the parameters we are considering here, where beside  $\tilde{t}_1$  only h and the LSP are light, the only decay mode of  $\tilde{t}_1$  is into  $c\chi^0$ . An analysis of signatures and background for the stop pair production including the decay mode we are considering already exists[25]. This issue is also important for the extraction of mass and mixing angle in the pair production. Furthermore for the precise measurements of these parameters the question of radiative corrections needs to be taken into account. All the results presented here correspond to a rather large value for  $\mu$  ( $\mu = 400GeV$ ), different values of  $\mu$  could lead to a different MSSM spectrum and eventually different decay modes for the  $\tilde{t}_1$ . This could even facilitate the extraction of the signal. However for the production process itself, the numerical results would not differ much in the region that is most interesting, the large mass splitting region, since the contribution from the  $\mu$  term to the vertex is small compared with the trilinear coupling contribution. Here we have used only one-loop corrections to  $M_h$ , the inclusion of the dominant two-loop corrections[2] should not affect the results very much as in associated



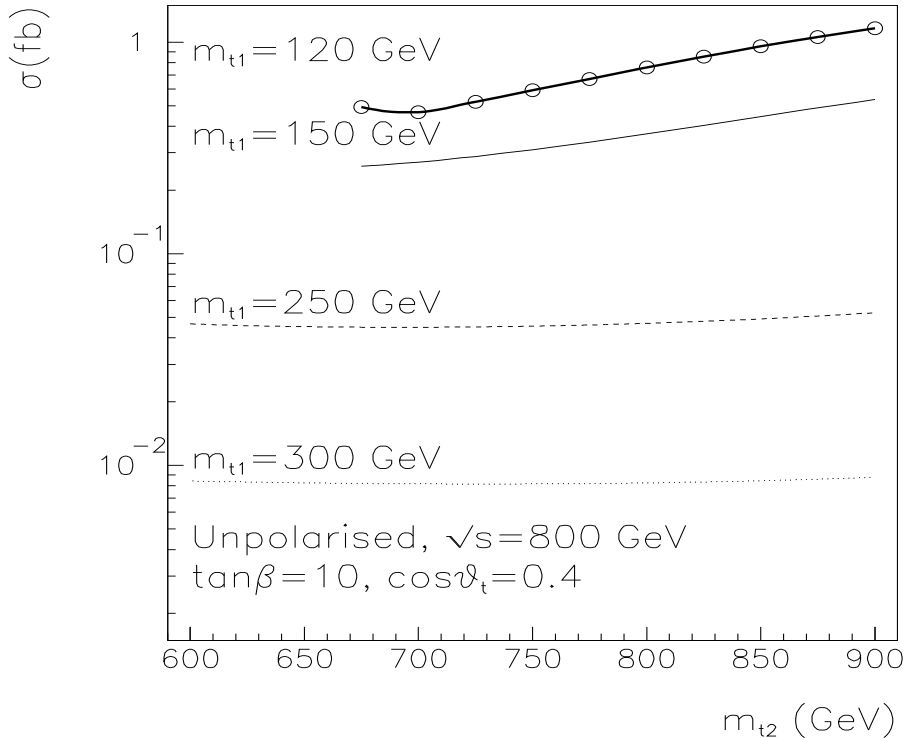


Figure 8: *Cross-section for  $e^+e^- \rightarrow \tilde{t}_1\tilde{t}_1Z$  at 800GeV for  $m_{\tilde{t}_1} = 120, 150, 250, 300\text{GeV}$ ,  $\cos\theta_{\tilde{t}} = 0.4$ ,  $\tan\beta = 10$  and  $\mu = 400\text{GeV}$ .*

Z production, we have found very little dependence on the precise value of the Higgs mass.

In conclusion, the process  $e^+e^- \rightarrow \tilde{t}_1\tilde{t}_1Z$  should be measurable at a high luminosity linear collider such as TESLA, provided the  $\tilde{t}_1$  is not very far above the present limit. While observable for any values of the parameters, (our conclusion applies to the small  $\tan\beta$  regime), this process can give additional information on the not directly observable  $m_{\tilde{t}_2}$  provided there is large mixing and mass splitting. In this sense it is very similar to  $\tilde{t}_1\tilde{t}_1h$ . There are regions in parameter space where only the  $\tilde{t}_1\tilde{t}_1Z$  would be observable. In this worst-case situation, even though the cross-section does not depend strongly on the parameters, one can still get a rough determination of a range for  $m_{\tilde{t}_2}$ . For the intermediate mixing we have discussed at length, non observation of  $\tilde{t}_1\tilde{t}_1h$  and a “low” value for  $\tilde{t}_1\tilde{t}_1Z$  would indicate a  $\tilde{t}_2$  in the 400-600 GeV range.

## References

- [1] See also, H. Haber and R. Hempfling, Phys. Rev. Lett. **66** (1991) 1815.  
 Y. Okada, M. Yamaguchi and T. Yanagida, Prog. Theor. Phys. **85** (1991) 1.  
 R. Barbieri and M. Frigeni, Phys. Lett. **B 258** (1991) 395. **B262** (1991) 477.
- [2] S. Heinemeyer, W. Hollik and G. Weiglein, Phys. Rev. **D58** (1998) 091701, hep-ph/9803277; *ibid*, Phys. Lett. **B440** (1998) 296, hep-ph/9807423; *ibid* hep-ph/9812472; *ibid* hep-ph/9903404.  
 The limiting case of vanishing stop mixing and large  $M_A$  and  $\tan\beta$  has been considered by R. Hempfling and A. Hoang, Phys. Lett. **B331** (1994) 99.
- [3] H. Baer, M. Bisset, C. Kao and X. Tata, Phys. Rev. **D46** (1992) 1067.  
 B. Kileng, Z. Phys. **C63** (1993) 87.  
 B. Kileng, P. Osland, P.N. Pandita, Z.Phys. **C71** (1996)87. hep-ph/9506455.  
 G. L Kane, G. D. Kribs, S.P Martin and J. D. Wells, Phys. Rev. **D50** (1996) 213.  
 A. Djouadi, Phys.Lett. **B435** (1998) 101. hep-ph/9806315.
- [4] G. Bélanger, F. Boudjema and K. Sridhar, hep-ph/9904348.
- [5] For a study of stop stop Higgs production at the LHC see, A. Djouadi, J. L. Kneur and G. Moultaka, Phys. Rev. Lett. **80** (1998) 1830. hep-ph/9711244.
- [6] A. Dedes and S. Moretti, preprint RAL-TR-1998-081, Dec. 1998.hep-ph/9812328; *ibid* RAL-TR-1999-033, hep-ph/9904491.
- [7] A. Djouadi, J. L. Kneur and G. Moultaka, hep-ph/9903218.
- [8] S. Dimopoulos and G. F. Giudice, Phys. Lett. **357** (1995) 573.  
 A. Pomarol and D. Tommasini, Nucl. Phys. **B466** (1996) 3.  
 G. Dvali and A. Pomarol, Phys. Rev. Lett. **77** (1996) 3728; *ibid* Nucl. Phys. **B522** (1998) 3.  
 A. G. Cohen, D.B. Kaplan and A. E. Nelson, Phys. Lett. **B388** (1996) 588.  
 J.L. Feng, C. Kolda and N. Polonsky, hep-ph/9810500.
- [9] N. Arkani-Hamed and H. Murayama, Phys. Rev. **D56** (1997) 6733.  
 K. Agashe and M. Graesser, Phys.Rev. **D59** (1999) 15007. hep-ph/9801446.
- [10] See for instance, J. R Espinosa, Nucl. Phys. **B475** (1996) 273.  
 J.M. Cline, M. Joyce and K. Kainulainen, Phys. Lett. **B417** (1998) 79. hep-ph/9708393.  
 M. Carena, M. Quirós and C.E.M. Wagner, Nucl. Phys. **B524** (1998) 3. hep-ph/9710401.  
 J.M. Moreno, M. Quirós and M. Seco, Nucl. Phys. **B526** (1998) 489. hep-ph/9801272.

- M. Laine and K. Rummukainen, Phys. Rev. Lett. **80** (1998) 5259. hep-ph/9804255.  
J.M. Cline, Preprint McGill-98/27. hep-ph/9810267.
- [11] See for instance, E. Accomando et al., Phys. Rep. **299** (1998) 1. hep-ph/9705442.
- [12] A. Bartl et al., Z. Phys. **C76** (1997) 549, hep-ph/9701336.
- [13] A. Bartl *et al.*, hep-ph/9709252.
- [14] G. Bélanger, F. Boudjema, T. Kon and V. Lafage, hep-ph/9811334, Eur. J. Phys.,  
in Press.
- [15] S. Kraml, Talk given at the ECFA Workshop on Physics at linear collider, Oxford,  
March 1999.  
H. Eberl, Talk given at the ECFA Workshop on Physics at linear collider, Sitges,  
April 1999.
- [16] A. Djouadi *et al.*, Phys. Rev. Lett. **78** (1997) 3626; Phys. Rev. **D57** (1998) 4179.
- [17] J. Erler and P. Langacker, hep-ph/9809352.
- [18] J. Ellis and G. Ridolfi and F. Zwirner, Phys. Lett. **B262** (1991) 477.
- [19] J.M. Frère, D.R.T Jones and S. Raby, Nucl. Phys. **B222** (1983) 11.  
M. Claudson, L. Hall and I. Hinchcliffe, Nucl. Phys. **B228** (1983) 501.  
C. Kounnas, A.B. Lahanas, D.V. Nanopoulos and M. Quirós, Nucl. Phys. **B236**  
(1984) 438.  
J.F. Gunion, H.E. Haber and M. Sher, Nucl. Phys. **B306** (1988) 1.  
P. Langacker and N. Polonsky, Phys. Rev. **D50** (1994) 5824.  
A. Strumia, Nucl. Phys. **B482** (1996) 24.  
For a recent summary see, J. A. Casas, to be published in *Perspectives on Supersym-*  
*metry*, ed. G. L. Kane, World scientific. hep-ph/9707475.
- [20] A. Kusenko, P. Langacker and G. Segre, Phys. Rev. **D54** (1996) 5824. hep-  
ph/9602414.  
A. Kusenko and P. Langacker, Phys. Lett. **391** (1997) 29. hep-ph/9608340.  
A. Kusenko, Nucl. Phys. Proc. Suppl. **52A** (1997) 67. hep-ph/9607287.
- [21] The limit on the mass of the SUSY Higgs depends on the SUSY parameters. For an  
update on the limits on the Higgs mass see:  
F. Gianotti, Opal talk for the LEP Committee, March 1999,  
[http://alephwww.cern.ch/ALPUB/seminar/lepc\\_mar99.pdf](http://alephwww.cern.ch/ALPUB/seminar/lepc_mar99.pdf).

N.J. Kjaer, Delphi talk for the LEP Committee, March 1999,  
<http://delphiwww.cern.ch/delfigs/figures/niels990324.ps.gz>.

G. Bobbink, L3 talk for the LEP Committee, March 1999,  
[http://l3www.cern.ch/conferences/ps/Bobbink\\_LEPC9903.ps](http://l3www.cern.ch/conferences/ps/Bobbink_LEPC9903.ps).

D. A. Glenzinski, Opal talk for the LEP Committee, March 1999,  
<http://www1.cern.ch/Opal/plots/glenzinski/main.ps.gz>.

[22] Aleph Collaboration, Phys. Lett. **434** (1999) 189. hep-ex/9810028.

[23] For a description of the program see for example M. Jimbo and H. Tanaka and T. Kaneko and T. Kon, hep-ph/9503363.

J. Fujimoto et al., Comp. Phys. Commun. **111** (1998) 185. hep-ph/9711283.

[24] H. Eberl, S. Kraml, W. Majerotto, **JHEP**9905 (1999) 016. hep-ph/9903413.

[25] A. Bartl and W. Majerotto, Talk given at the *European Pre-meeting on  $e^+e^-$  Collisions at 500 GeV*, DESY Hamburg, April 2-3, 1993.